

The metamorphic evolution of mafic rocks in the Tugela Terrane, Natal Belt, South Africa

A. Bisnath

Council for Geoscience, Pietermaritzburg, South Africa
Present Address: Kai Batla Minerals Industry Consultants, P.O.Box 41955, Craighall, 2024,
Gauteng, South Africa
e-mail: abisnath@kaibatla.co.za

S. McCourt

School of Geological Sciences, University of KwaZulu-Natal (Westville Campus) Durban, South Africa.
e-mail: mccourts@ukzn.ac.za

H.E Frimmel

Department of Geological Sciences, University of Cape Town, Rondebosch 7701, South Africa
Present Address: Division for Geodynamics and Geomaterials Research, Institute of Geography,
University of Würzburg, Am Hubland, D-97074, Würzburg
e-mail: hartwig.frimmel@uni-wuerzburg.de

S.B.N. Buthelezi

School of Geological Sciences, University of KwaZulu-Natal (Westville Campus) Durban, South Africa.
Present Address: Kai Batla Minerals Industry Consultants, P.O.Box 41955, Craighall, 2024, Gauteng, South Africa
e-mail: sbuthelezi@kaibatla.co.za

© 2008 December Geological Society of South Africa

ABSTRACT

New petrological and mineral chemical data indicate a clockwise P-T path for medium- to high-grade metamorphic mafic rocks in different thrust sheets of the Tugela Terrane within the Mesoproterozoic Natal Belt in KwaZulu-Natal (eastern South Africa). Three metamorphic stages are distinguished: (i) an early upper amphibolite- to lower granulite-facies metamorphic event (M_1) is indicated by rare relics of clinopyroxene; (ii) mineral chemical and textural equilibration during M_2 at calculated pressure-temperature conditions of 4.5 to 6 kbar and 693 to 750°C; and (iii) partial diffusional resetting of mineral compositions during subsequent uplift and exhumation (M_3) under lower amphibolite- to greenschist-facies conditions. No major differences were noted in the tectono-thermal regimes at which each of the respective thrust sheets were deformed suggesting that the Tugela Terrane was a homogenous package and experienced uniform P-T conditions. The new data acquired in this study contribute to an improvement in the ongoing development of a tectono-thermal and geodynamic model for the Natal Belt.

Introduction

KwaZulu-Natal in eastern South Africa contains a Mesoproterozoic orogenic belt that provides useful information for the understanding of both the amalgamation and fragmentation of supercontinents towards the end of the Mesoproterozoic at *c.* 1.2 to 1.0 Ga. The Mesoproterozoic Natal Belt of southern Africa lies adjacent to the southeastern margin of the Kaapvaal Craton and is truncated to the east against the Indian Ocean margin of the African continent. The Natal Belt is divided, from north to south, into the Tugela, Mzumbe and Margate Terranes (Thomas, 1989; Johnston *et al.*, 2003; Figure 1). The Mzumbe and Margate Terranes are characterised by voluminous 1.2 to 1.0 Ga granitoid gneisses that have been interpreted as deeply eroded magmatic arcs (Thomas, 1989; Thomas *et al.*, 1993; 1999). Published tectonic models assume that the Mzumbe and Margate Terranes are magmatic arcs that developed in response to Mesoproterozoic ocean basin closure south of the Kaapvaal Craton with subduction away from the craton (Matthews, 1972; 1981;

Jacobs *et al.*, 1993; Jacobs and Thomas, 1994; Thomas *et al.*, 1994).

In contrast to the Margate and Mzumbe Terranes, the Tugela Terrane consists of a heterogeneous assemblage of amphibolite-facies mafic and felsic orthogneisses, layered mafic and ultramafic complexes and metasedimentary rocks. The ultramafic rocks present in the Tugela Terrane and its intermediate position between the Kaapvaal Craton and southern arc terranes prompted Matthews (1972; 1981) to suggest that the Tugela Terrane represents part of a Mesoproterozoic ophiolite that was obducted onto the Kaapvaal Craton during Mesoproterozoic orogeny. Recent mapping (Bisnath, 2000; Johnston *et al.*, 2003) and geochemical studies (Arima *et al.*, 2001) have shown that the Tugela Terrane consists of several thrust sheets each of which has a distinct tectono-magmatic signature. These authors interpreted the Tugela Terrane as an accretionary complex consisting of rocks formed in an intra-oceanic island arc and oceanic island settings that subsequently accreted to the continental margin of the Kaapvaal Craton.

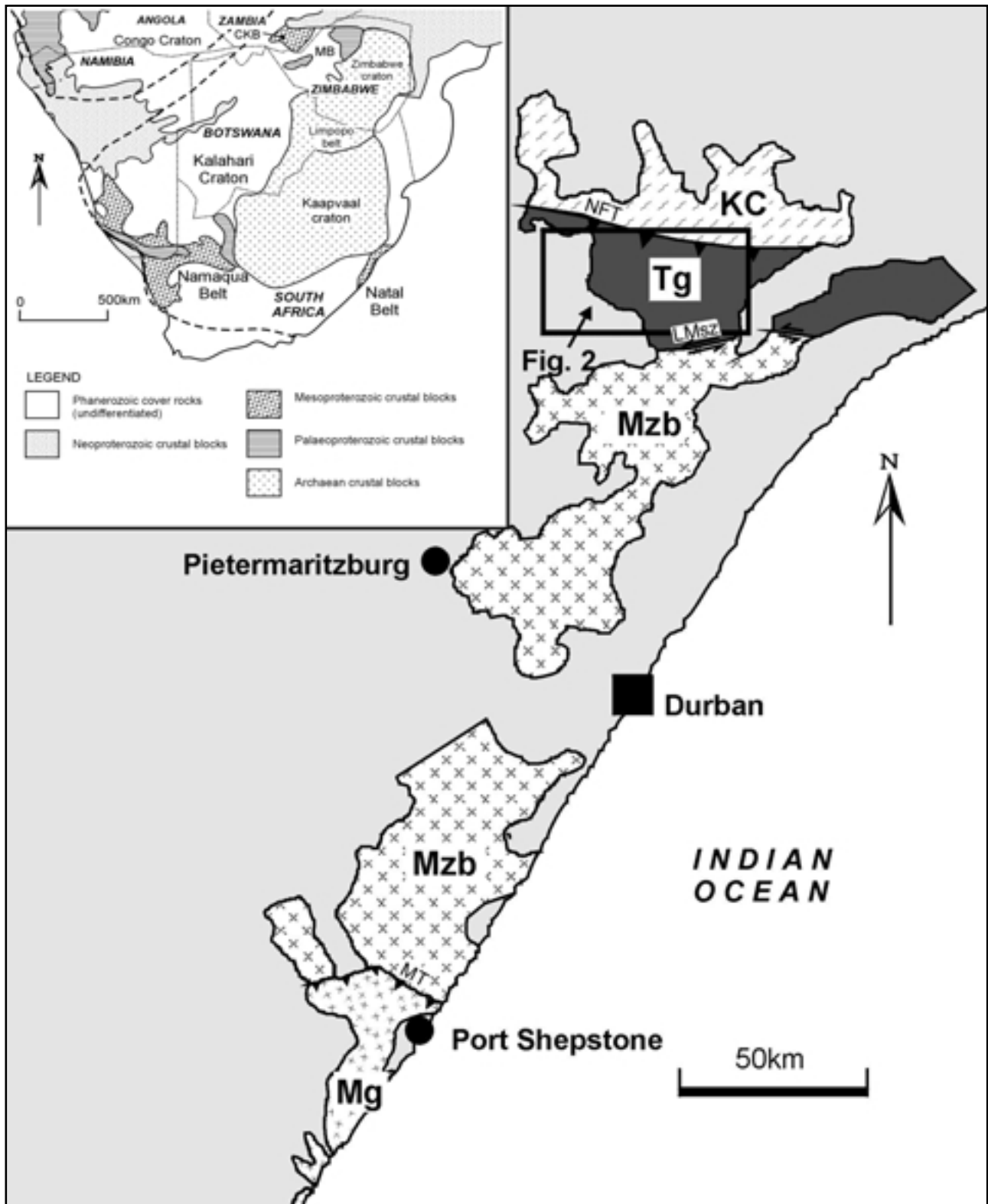


Figure 1. Simplified geological map of the Natal belt showing the distribution and relative positions of the Margate, Mzumba and Tugela terranes (after Thomas *et al.*, 1993) and the principal localities mentioned in the text. For reference KC refers to Kaapvaal craton and NFT to Natal thrust front. On the insert, simplified map to illustrate the principal elements in the tectonic framework of southern Africa. For reference MB indicates the Palaeoproterozoic Magondi belt in Zimbabwe and CKB indicates the Mesoproterozoic Choma-Kalomo block in Zambia. The block of Archaean crust comprising, from south to north, the Kaapvaal craton, Limpopo belt and Zimbabwe craton.

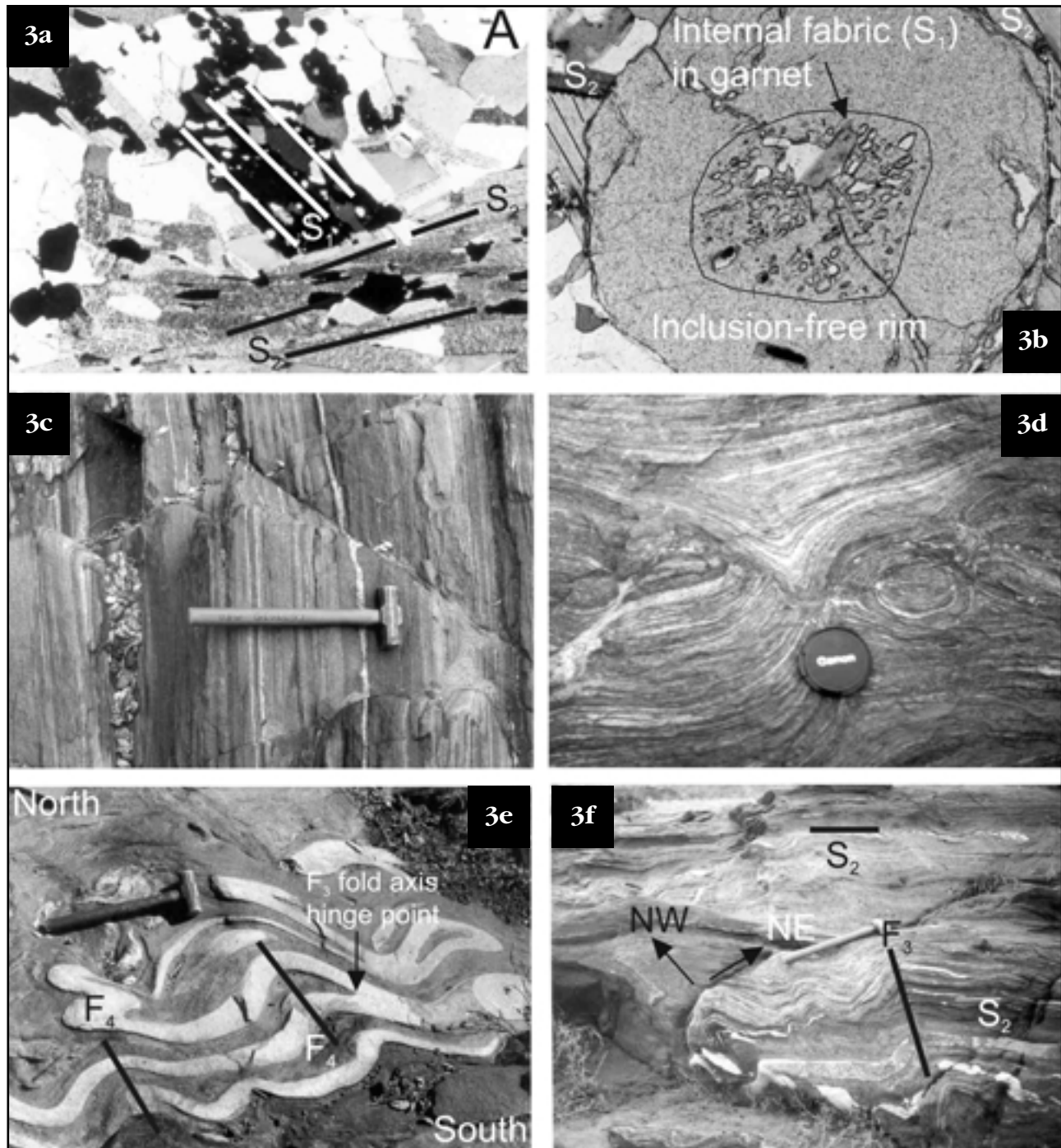


Figure 3. (a) Photomicrograph of discordant relationship between S_1 and S_2 foliations. Note the angle of approximately 45° between the inclusions trails in garnet (S_1) and the biotite laths (S_2); (b) Photomicrograph of garnet with quartz, feldspar and biotite inclusions truncated by an inclusion free rim; (c) The dominant S_2 planar fabric defined by compositional banding; (d) Scar folds related to boudinage of S_2 ; (e) Fold interference pattern (Type 3) due to two sets of coaxial F_3 and F_4 folds deforming S_2 ; (f) Field photo of F_3 folds deforming the dominate S_2 foliation.

In this contribution, the tectono-thermal regimes in which the rocks defining the thrust sheets of the Tugela Terrane were deformed and metamorphosed are assessed. In order to resolve the complex tectono-thermal history of the area, detailed petrographic and geothermobarometric studies were carried out on mafic rocks to generate, in conjunction with published geochronological data (Bisnath, 2000; Johnston *et al.*, 2001; McCourt *et al.*, 2006), a coherent pressure-

temperature (P-T) path and an improved geodynamic model for this part of the Natal Belt.

Geology of the Tugela Terrane

Mathews (1981) defined the Tugela Terrane as an ophiolitic, west-plunging thrust stack that consists of four thrust sheets or nappes named, from east to west and bottom to top, the Nkomo, Madidima, Mandleni and Tugela Nappes (Figure 2). He interpreted the



Figure 4. Photograph of a roadcut showing fold interference pattern (Type 3) due to two sets of coaxial F_3 and F_4 folds deforming S_2 .

dismembered ultramafic lenses and associated talc schist distributed throughout the Tugela Terrane as defining the contacts between thrust sheets. Matthews (1972; 1981) regarded the rocks of the Tugela thrust sheet as the most oceanic in character and thus interpreted them as the most allochthonous. The rocks defining the Nkomo thrust sheet were considered to be para-autochthonous and thought to be linked to the margin of the Kaapvaal Craton. In the Nkomo and Madidima thrust sheets, quartzo-feldspathic gneiss is the dominant lithology with subordinate amounts of metasedimentary rocks and amphibolite, whereas the Mandleni and Tugela thrust sheets consist of bimodal meta-igneous rocks.

Tugela thrust sheet

The Tugela thrust sheet (TTS) is dominated by the Manyane amphibolite, comprising amphibolite, amphibole gneiss and tremolite-chlorite schist, and the Kotongweni meta-tonalite (Harmer, 1979). The latter is a homogeneous tonalitic garnet hornblende gneiss that is intrusive into the Manyane amphibolite (Johnston *et al.*, 2003; McCourt *et al.*, 2006). Minor amounts of felsic gneiss, layers of magnetite quartzite and dolomite are sparsely interfoliated with the mafic rocks. Arima *et al.*

(2001) demonstrated that the Manyani amphibolites were derived from low-K tholeiitic basaltic rocks and the Kotongweni tonalite is an extremely depleted M-type granitoid, with low abundances of K, Rb, rare earth elements (REE's) and large ion lithophile elements (LILE), similar to rocks forming in the present day Izu-Bonin arc. Arima *et al.* (2001) therefore interpreted the Kotongweni tonalite and the Manyani amphibolite as the volcanic and plutonic components of a Mesoproterozoic ocean arc system. Within the TTS, four plutonic bodies have been identified. These are the ultramafic/mafic Tugela Rand and Macala complexes, the Mkondene diorite and the Dimane granite.

McCourt *et al.* (2006) reported that the medium- to coarse-grained Mkondene meta-diorite is also intrusive into the Manyane amphibolite. The typical mineralogy is biotite, hornblende, plagioclase and quartz. Orthopyroxene is locally present. Regional mapping indicates that with increasing strain and thus foliation intensity, the orthopyroxene-bearing diorite grades into biotite-hornblende gneiss (Harmer, 1979)

The Tugela Rand Complex (Wilson, 1990) comprises an association of layered mafic and ultramafic rocks that are characterised by well preserved primary magmatic structures. An informal subdivision of the intrusive body

Table 1. Subdivision of the Tugela Terrane in the study area listing thrust sheets and the amphibolitic units within them (compiled from Matthews and Charlesworth, 1981; Thomas, 1989b; Bisnath, 2000).

Thrust Sheet	Amphibolitic Unit	Description
Tugela	Manyane Amphibolite	Medium to coarse grained, green coloured rock. Commonly folded together with feldspathic gneiss hbl+pl+qtz+bt±ep±opaque Intruded by Mkhondeni Diorite and Tugela Rand Complex
Mandleni	Wosi Amphibolite	Medium to coarse grained, dark green rock. Folded with aplitic dykes and feldspathic gneiss hbl+pl+qtz+grt±ep±bt±opaque Intruded by Mambulu Complex
Madidima	Undifferentiated Amphibolite	Medium to coarse grained dark green rock. hbl+pl+grt+qtz±ep±bt±opaques Intruded by numerous granitoid dykes
Nkomo	Khomo Amphibolite	Dominantly coarse grained dark green rock. bt+hbl+pl+qtz+opaque Folded with feldspathic gneiss and aplitic dykes

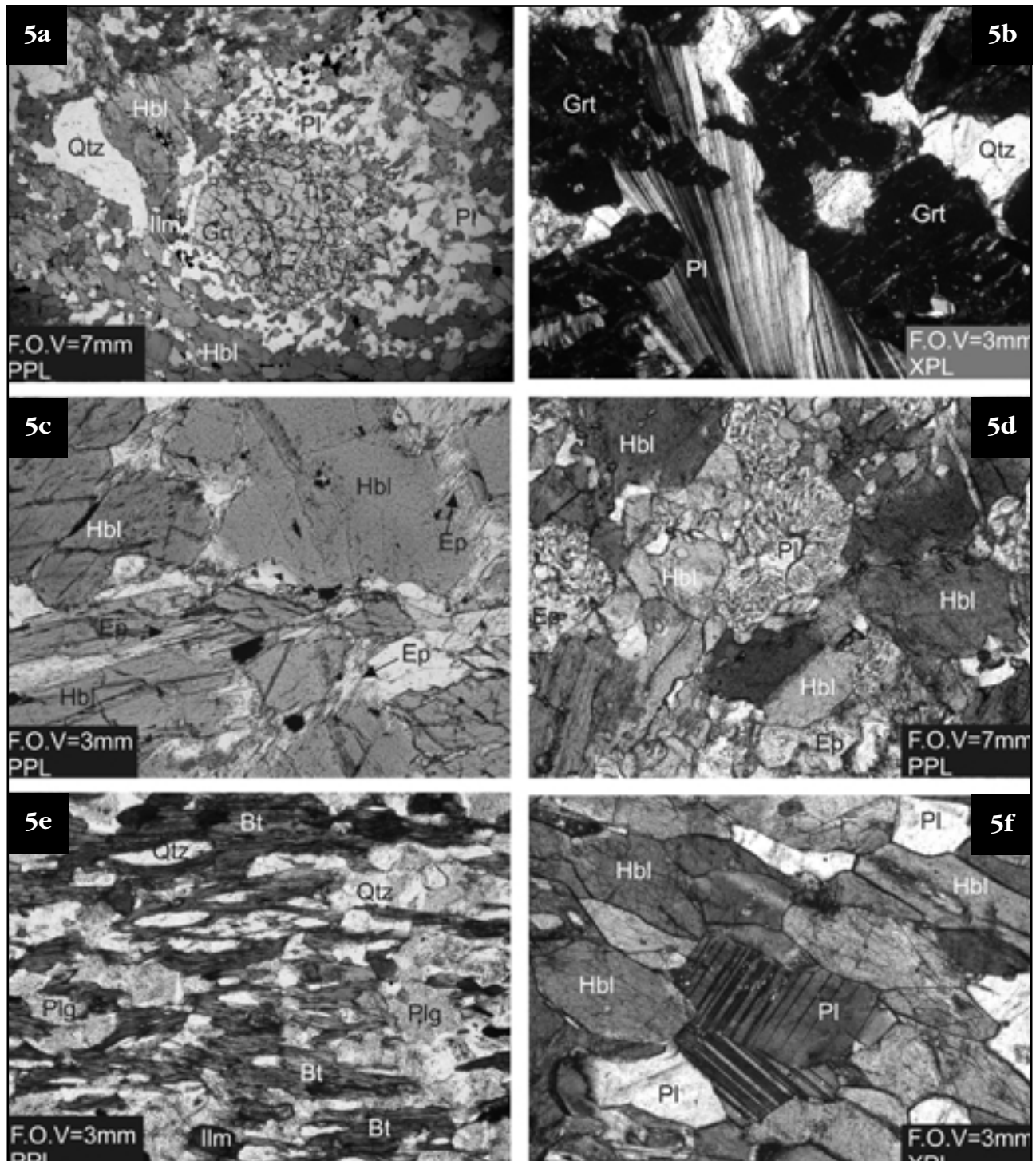


Figure 5. (a) Fragmented garnet with corona of quartz (Qtz) and plagioclase (Pl) surrounded by green hornblende (Hbl); (b) Radiating plagioclase twins within cracks in a garnet; (c) Epidote (Ep) replacing hornblende along grain boundaries; (d) Symplectic corona of epidote around plagioclase; (e) Laths of biotite enclosing lens of quartz. Note the cloudy nature of plagioclase due to sericitization; (f) Wedged-shaped deformation twins within plagioclase.

by Wilson (1990) recognises seven lithological zones with bronzitite at the base and troctolite at the top. Serpentinised wehrlite and gabbroids are the most common rock types. The Tugela Rand Complex is intrusive into both the Manyane amphibolites and the Mkondene meta-diorite and is, in turn, intruded by the Dimane granite (Wilson, 1990). It has been

suggested that the complex may represent the roots of an oceanic island (see McCourt *et al.*, 2006).

McCourt *et al.* (2006) also reported that the Dimane granite outcrops along the western margin of the Tugela Rand Complex, where it is discordant to gabbro, pyroxenite and serpentinite (Harmer, 1979). The granite is medium-grained, equigranular and composed of

quartz, microcline and minor biotite (Harmer, 1979). Although the granite is typically massive, a non-penetrative foliation defined by biotite is locally developed. Harmer (1979) noted the common occurrence of both veined and massive amphibolite xenoliths in the Dimane granite.

Mandleni thrust sheet

The Mandleni thrust sheet (MTS) is structurally below the TTS and is underlain by the Dondwana gneiss unit comprising both amphibolitic and leucocratic feldspathic gneiss with the mafic component referred to as the Wozi amphibolite. From geochemical data, Johnston *et al.* (1998) and Arima *et al.* (2001) have suggested that the Dondwana gneiss unit represents a deformed and metamorphosed bimodal magmatic sequence formed in an oceanic island setting. The MTS contains two igneous complexes; the ultramafic Sithilo, and the layered gabbroic Mambula complex. The Sithilo complex comprises talc-schist and serpentinitised lenses of harzburgite with local occurrences of podiform chromitite (Johnston *et al.*, 2003 and references therein) whereas the Mambula complex consists of gabbro, pyroxenite, massif-type anorthosite and it is host to sub-economic deposits of titaniferous magnetite (Reynolds, 1986).

Madidima thrust sheet

The Madidima thrust sheet (MDTS) is dominated by the Dulumbe paragneiss (Johnston *et al.*, 2001), which is a thick succession of homogeneous biotite gneiss. The Dulumbe paragneiss forms the structurally highest portion of the MDTS and grades downwards into a heterogeneous succession of garnet-biotite, garnet-biotite-sillimanite and muscovite-biotite schists, calc-silicate gneiss with minor amounts of amphibolite, graphite schist and marble. This structurally lower unit is referred to as the Gazeni metasedimentary sequence (Matthews and Charlesworth, 1981; Bisnath, 2000).

Nkomo thrust sheet (NTS)

The Nkomo thrust sheet (NTS) is the structurally lowest thrust sheet and is overlain by the MDTS. This package consists of two mappable units, *i.e.*, the Halambu granitoid gneiss unit and the Khomo amphibolite unit (Smalley, 1980). The Halambu granitoid gneiss unit is a uniform grey, medium- to coarse-grained, foliated rock of granodioritic to tonalitic composition and it is characterised by an abundance of amphibolitic xenoliths (Smalley, 1980). The Khomo amphibolite comprises interbanded amphibolitic gneisses, schists and aplite dykes. The regional foliation of the Khomo amphibolite unit is concordant with that of the Halambu granitoid gneiss unit. The Khomo amphibolites are fine- to medium-grained, compositionally layered and contain lenses and layers of quartzo-feldspathic material giving the rock a streaky appearance.

Structural Geology

No primary structures were observed in the gneissic rocks of the Tugela Terrane and it is concluded that the penetrative deformation and recrystallisation during syn-kinematic metamorphism has transposed all primary features. We recognise four planar tectonic fabrics (S_1 - S_4) and one linear fabric. The oldest fabric (S_1) is poorly preserved and has largely been overprinted by subsequent deformation. At outcrop scale, rare detached isoclinal intrafolial folds that deformed compositional layering can be observed (Johnston *et al.*, 2003). The S_1 fabric has also been recognised as an internal fabric in garnet and either truncates against garnet margins (Figure 3A) or against an inclusion-free marginal zone within the garnet porphyroblasts (Figure 3B).

The dominant S_2 planar fabric, a penetrative axial planar cleavage, is parallel to lithological contacts and is defined by compositional banding (Figure 3C) and by the alignment of coarse mineral grains throughout the Tugela Terrane. Isoclinal intrafolial folds of S_1 indicate that S_2 developed in response to isoclinal folding and transposition of older contacts (D_2 ; Johnston *et al.*, 2001). On a regional scale S_2 is deformed by open to tight, northeast-verging F_3 folds with fold axes that trend 120 - 300° and very open F_4 folds. Locally the S_2 foliation is deformed into sharply defined wave-like structures. These are scar-folds related to the development of boudinage in slightly more competent layers (Figure 3D). Planar fabrics and folds attributable to the multiple deformation events are recognisable at map scale (see Bisnath, 2000; Johnston *et al.*, 2003) and at outcrop scale where they result in spectacular Type-3 interference patterns (after Ramsay, 1967; Figure 3E). The presence of northeast-vergent F_3 folds, map-scale nappes, rotated boudins and extensional shear bands (Figure 3F) suggests that D_3 was characterised by ductile deformation during top-to-north shearing (Johnston *et al.*, 2001).

The D_3 event is characterised by the folding and faulting of the S_2 fabric (Figure 4). The F_3 folds are generally tight, have thickened hinges, and are asymmetric verging to the northeast. Syn-kinematic lower amphibolite-facies metamorphism resulted in retrograde overprinting of the S_2 fabric. This S_3 fabric is orientated at a high angle to the S_2 fabric in F_3 fold hinges, whereas the S_3 parallels the S_2 in the long limbs of the F_3 folds. Locally the lower limbs and cores of these folds are cut by sub-horizontal to southwest dipping, northeast verging thrust faults. These faults are parallel to the axial surface of F_3 folds.

Metamorphic History

Felsic orthogneiss and semipelitic paragneiss from the MDTS are dominated by feldspar, quartz, biotite, garnet and locally hornblende. The pelitic gneiss of the MDTS consists of garnet, biotite, feldspar, quartz and sillimanite. These mineral assemblages provide limited constraints on the pressure and temperature conditions

Table 2. Representative electron microprobe results for hornblende-plagioclase pairs.

Sample #	SB01		SB06		SB24		SB17		SB07A		SB31	
	28°58.181'S	31°07.918'E	28°57.036'S	31°02.330'E	28°51.612'S	31°00.696'E	28°46.604'S	30°54.507'E	28°53.754'S	31°01.485'E	28°53.175'S	31°08.745'E
Grain #	Hbl 1	Hbl 17	Hbl 17	Hbl 22	Hbl 1	Hbl 26	Hbl 1	Hbl 7	Hbl 13	Hbl 22	Hbl 8	Hbl 2
SiO ₂	44.26	43.35	44.41	45.41	44.76	44.79	43.61	43.18	41.54	42.30	45.77	46.98
TiO ₂	0.81	0.85	1.18	1.06	0.57	0.57	0.64	0.66	0.64	0.71	0.42	0.38
Al ₂ O ₃	11.36	12.43	12.23	11.02	11.99	10.87	11.50	11.58	11.48	11.71	10.38	8.97
Cr ₂ O ₃	0.01	0.01	0.01	0.00	0.03	0.06	0.02	0.01	0.08	0.08	0.01	0.02
FeO	15.84	16.26	16.51	14.40	15.38	14.84	17.48	17.66	19.61	19.08	14.38	13.05
MnO	0.29	0.29	0.17	0.08	0.21	0.30	0.31	0.29	0.39	0.39	0.34	0.32
MgO	11.30	10.96	9.98	12.07	11.35	11.90	10.08	9.81	9.22	8.88	12.58	13.74
CaO	12.62	12.53	11.21	12.26	12.52	12.66	12.32	12.24	11.67	12.39	12.64	12.06
Na ₂ O	1.17	1.31	1.49	1.18	1.31	1.26	1.51	1.48	1.46	1.56	1.05	0.88
K ₂ O	0.33	0.36	0.45	0.37	0.26	0.21	0.40	0.39	0.88	0.80	0.54	0.42
Total	97.98	98.36	97.64	97.86	98.37	97.46	97.85	97.30	96.95	97.90	98.11	96.82
Si	6.49	6.34	6.52	6.61	6.52	6.58	6.48	6.45	6.27	6.38	6.66	6.82
Al (vi)	1.51	1.66	1.48	1.39	1.48	1.42	1.52	1.55	1.73	1.62	1.34	1.18
T	8.00	8.00	8.00	8.00	8.00	8.00	8.00	8.00	8.00	8.00	8.00	8.00
Al (iv)	0.46	0.49	0.64	0.50	0.57	0.46	0.49	0.49	0.32	0.46	0.44	0.36
Ti	0.09	0.09	0.13	0.12	0.06	0.06	0.07	0.07	0.07	0.08	0.05	0.04
Cr	0.00	0.00	0.00	0.00	0.00	0.01	0.00	0.00	0.01	0.01	0.00	0.00
Fe(iii)	0.51	0.61	0.54	0.43	0.46	0.44	0.46	0.48	0.88	0.38	0.48	0.65
Fe(ii)	1.44	1.38	1.48	1.32	1.41	1.38	1.71	1.72	1.60	2.03	1.27	0.93
Mn	0.04	0.04	0.02	0.01	0.03	0.04	0.04	0.04	0.05	0.05	0.04	0.04
Mg	2.47	2.39	2.18	2.62	2.46	2.61	2.23	2.19	2.08	2.00	2.73	2.97
C	5.00	5.00	5.00	5.00	5.00	5.00	5.00	5.00	5.00	5.00	5.00	5.00
Ca	1.98	1.96	1.76	1.91	1.95	1.99	1.96	1.96	1.89	2.00	1.97	1.88
Na	0.02	0.04	0.24	0.09	0.05	0.01	0.04	0.04	0.11	0.00	0.03	0.12
B	2.00	2.00	2.00	2.00	2.00	2.00	2.00	2.00	2.00	2.00	2.00	2.00
Na	0.32	0.34	0.19	0.25	0.32	0.35	0.39	0.39	0.32	0.46	0.27	0.12
K	0.06	0.07	0.08	0.07	0.05	0.04	0.08	0.07	0.17	0.15	0.10	0.08
A	0.38	0.40	0.27	0.31	0.37	0.39	0.47	0.46	0.49	0.61	0.37	0.20
Total	15.38	15.40	15.27	15.31	15.37	15.39	15.47	15.46	15.49	15.61	15.37	15.20

Grain #	Plag 1	Plag 7	Plag 10	Plag 15	Plag 1	Plag 6	Plag 2	Plag 8	Plag 8	Plag 3	Plag 3	Plag 1
SiO ₂	57.07	57.24	54.77	57.17	60.14	55.21	60.73	59.17	59.45	57.79	59.06	58.66
Al ₂ O ₃	25.29	27.00	25.87	25.07	24.15	26.68	24.51	26.04	25.61	26.37	25.79	26.90
FeO	0.09	0.16	3.08	0.18	0.22	0.21	0.12	0.20	0.10	0.07	0.09	0.11
CaO	8.12	8.39	8.77	8.34	6.31	9.79	5.52	7.22	6.90	7.64	7.36	7.25
Na ₂ O	6.97	6.74	5.54	7.28	7.99	5.98	8.20	7.29	7.38	7.02	7.99	7.53
K ₂ O	0.00	0.00	0.03	0.04	0.07	0.09	0.09	0.04	0.05	0.11	0.00	0.00
MgO	0.07	0.03	0.11	0.01	0.00	0.01	0.00	0.00	0.01	0.00	0.03	0.05
Total	97.61	99.56	98.18	98.10	98.87	97.97	99.17	99.97	99.50	98.99	100.33	100.49
Si	2.62	2.57	2.54	2.62	2.71	2.54	2.72	2.64	2.66	2.61	2.63	2.61
Al	1.37	1.43	1.41	1.35	1.28	1.44	1.29	1.37	1.35	1.40	1.35	1.41
Fe(ii)	0.00	0.01	0.12	0.01	0.01	0.01	0.00	0.01	0.00	0.00	0.00	0.00
Ca	0.40	0.40	0.43	0.41	0.30	0.48	0.26	0.35	0.33	0.37	0.35	0.34
Na	0.62	0.59	0.50	0.65	0.70	0.53	0.71	0.63	0.64	0.61	0.69	0.65
K	0.00	0.00	0.00	0.00	0.00	0.01	0.01	0.00	0.00	0.01	0.00	0.00
Mg	0.00	0.00	0.01	0.00	0.00	0.00	0.00	0.00	0.00	0.00	0.00	0.00
Total	5.01	5.00	5.01	5.03	5.00	5.01	4.99	4.99	4.99	5.00	5.04	5.01

Formula based on 23 oxygen for hornblende and 8 oxygen for plagioclase. All Fe reported as FeO

during metamorphism. More useful in this regard are the amphibolitic rocks, which consist of garnet, plagioclase, hornblende, ilmenite and biotite with occasional relics of clinopyroxene. Such mafic rocks are preserved in all four thrust sheets, with minor variations in composition

(Table 1). As these rock are considered to be extrusive (Matthews, 1972; 1981; Arima *et al.*, 2001; Johnston *et al.*, 2003) it is implicit that the protolith experienced the entire metamorphic history recorded in these amphibolitic rocks. Given the degree of metamorphism

Table 3. Representative electron microprobe analyses for garnets in the garnet amphibolite.

Sample #:	SB06				SB12			
Locality	28°57.036'S; 31°02.330'E				28°50.380'S; 31°03.830'E			
Grain #:	Grt 1	Grt 2	Grt 3	Grt 4	Grt 1	Grt 5	Grt 13	Grt 15
SiO ₂	37.48	37.52	37.89	38.16	37.62	37.52	37.66	36.60
TiO ₂	0.01	0.02	0.01	0.03	0.02	0.04	0.03	0.07
Al ₂ O ₃	21.04	21.23	21.25	21.46	21.16	20.83	21.18	20.73
FeO	27.52	25.96	27.95	27.75	30.45	30.68	29.91	30.34
MnO	0.68	0.88	0.64	0.48	2.01	1.90	2.97	2.24
MgO	4.07	3.47	4.49	5.09	4.18	4.47	3.13	4.18
CaO	8.57	9.84	8.20	7.92	5.30	4.76	5.50	4.92
Cr ₂ O ₃	0.00	0.00	0.01	0.03	0.05	0.02	0.00	0.00
Total	99.37	98.92	100.43	100.90	100.78	100.21	100.38	99.08
Si	2.98	2.99	2.98	2.97	2.97	2.98	2.99	2.95
Ti	0.00	0.00	0.00	0.00	0.00	0.00	0.00	0.00
Al	1.97	1.99	1.97	1.97	1.97	1.95	1.99	1.97
Fe	1.83	1.73	1.84	1.81	2.01	2.04	1.99	2.05
Mn	0.05	0.06	0.04	0.03	0.14	0.13	0.20	0.15
Mg	0.48	0.41	0.53	0.59	0.49	0.53	0.37	0.50
Ca	0.73	0.84	0.69	0.66	0.45	0.41	0.47	0.43
Na	0.00	0.00	0.00	0.00	0.00	0.00	0.00	0.00
K	0.00	0.00	0.00	0.00	0.00	0.00	0.00	0.00
Cr	0.00	0.00	0.00	0.00	0.00	0.00	0.00	0.00
Ni	0.00	0.00	0.00	0.00	0.00	0.00	0.00	0.00
Sum	8.04	8.02	8.04	8.04	8.04	8.04	8.01	8.06
Mg#	0.21	0.19	0.22	0.25	0.20	0.21	0.16	0.20
Py	15.62	13.57	16.98	19.13	15.95	17.09	12.23	16.06
Alm	59.25	56.87	59.35	58.48	65.17	65.73	65.67	65.45
Gro	23.64	27.61	22.30	21.38	14.53	13.05	15.48	13.60
Sp	1.49	1.95	1.37	1.02	4.36	4.13	6.61	4.88

Formula based on 12 for garnet. All Fe reported as FeO.

and recrystallisation, any sequence of metamorphic events prior the emplacement of the mafic rocks is probably no longer preserved. The amphibolite and amphibolitic gneiss are, therefore, the most suitable rock types for reconstructing the P-T conditions experienced by the Tugela Terrane. Samples were collected from each thrust sheet in order to compare and contrast the peak metamorphic conditions and mineral assemblages (Table 1) preserved in the mafic rocks and thereby establish whether the peak metamorphic conditions for each of the thrust sheets were the same.

Mineral Chemistry

Seven amphibolite samples representing the range of pre-tectonic amphibolites from the different thrust sheets in the Tugela Terrane were selected for mineral chemical analysis. Mineral chemical data were acquired by conventional microprobe analyses using a JEOL 733 electron probe at the Council for Geoscience, South Africa. The analyses were performed using an accelerating voltage of 15 kV, a beam current of 30 and 40 nA and an analysing spot size of 2 to 5 micrometer. Data reduction was carried out by an on-line Fortan programme supplied by JEOL (FZAFOC), which uses the absorption correction of Philibert (1963) and Heinrich (1968), the atomic number correction of Duncumb and

Reed (1968) and the fluorescence correction of Reed (1965). A range of internationally certified standards were employed. The counting time at the element peak positions was 10 seconds and 5 seconds at two symmetrical background positions with a lower detection limit of 0.05%. Mineral abbreviations used are from Kretz (1983). All Fe is expressed as Fe²⁺ unless otherwise stated.

Mineral analyses for two samples were determined using a Leica 440 Stereoscan scanning electron microscope (SEM), equipped with an INCA (OXFORD) energy dispersive system (EDS), which controls the analytical capacity of the instrument at the Council for Geoscience. With this instrument it is possible to acquire secondary, backscattered and cathodoluminescence electron images, X-ray EDS microanalysis and X-ray element maps. All specimens were polished and coated with carbon to provide a conductive highly polished surface for optimum imaging and X-ray microanalysis. Mineral chemistry was determined by means of spot analyses with the EDS. Backscatter imaging, element mapping and EDS analysis were done at a probe current of 2 nA, accelerating voltage 20 kV and counting time was set at 100 s. The default reference standards as supplied by Oxford's INCA software as well as own standards were used.

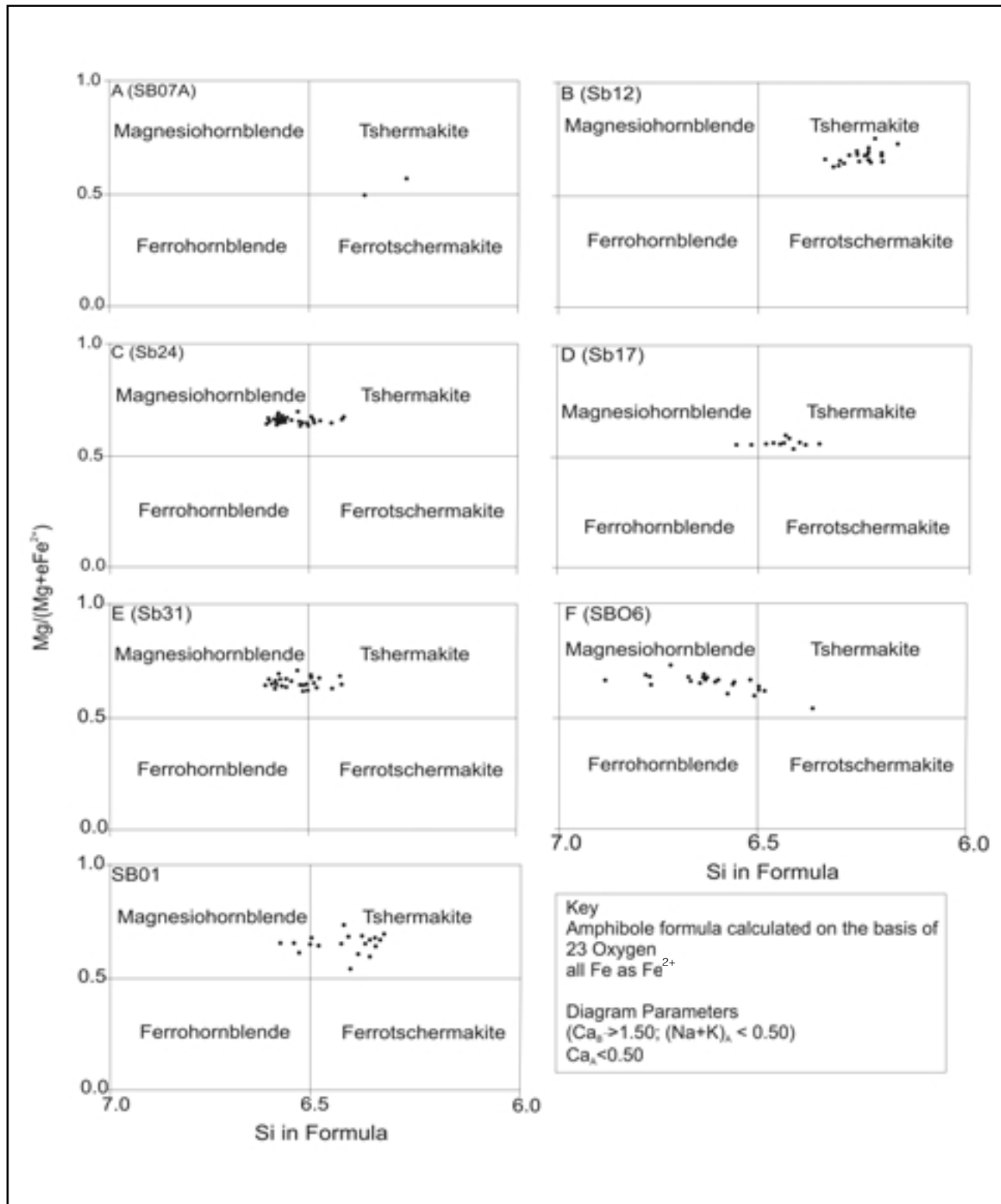


Figure 6. Amphibole classification for samples SB07A, SB12, SB24, SB17, SB31, SB06, SB01 according to the classification scheme of Leake *et al.* (1987).

Amphibolites

A variety of amphibolites were observed in the field. The rocks generally appear dark green to black and are well foliated resulting in a laminated/banded surface appearance. Primary mineral assemblages were largely obliterated as a result of metamorphism and deformation. Apart from relics of diopside, the

occasional presence of brown hornblende grains, perthitic potassium feldspar porphyroclasts and the replacement of biotite by potassium feldspar, the oldest preserved mineral assemblage is a re-equilibrated mineral assemblage that defines the S₂ fabric in the amphibolites. It consists of hornblende + plagioclase + quartz ± garnet ± biotite ± ilmenite. Secondary epidote,

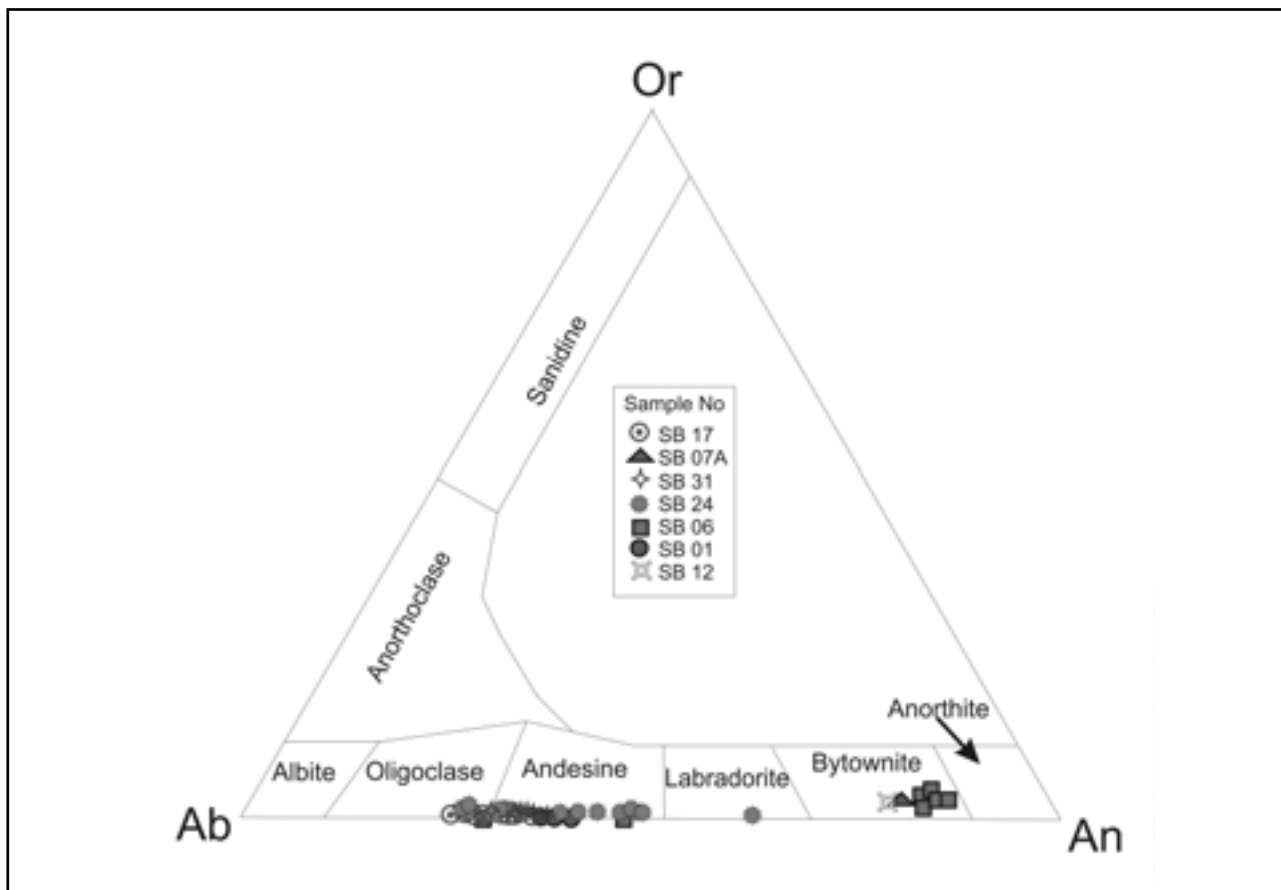


Figure 7. Plagioclase compositions in mafic meta-igneous rocks.

actinolite and sericite are ascribed to a retrograde overprint. Four varieties of amphibolites are distinguished:

1. garnet amphibolite;
2. epidote amphibolite;
3. biotite amphibolite; and
4. amphibolite.

The garnet amphibolite is characterised by red intensely deformed garnet porphyroblasts, 2 to 5 mm in diameter, that are interpreted as products of the unbalanced reaction:

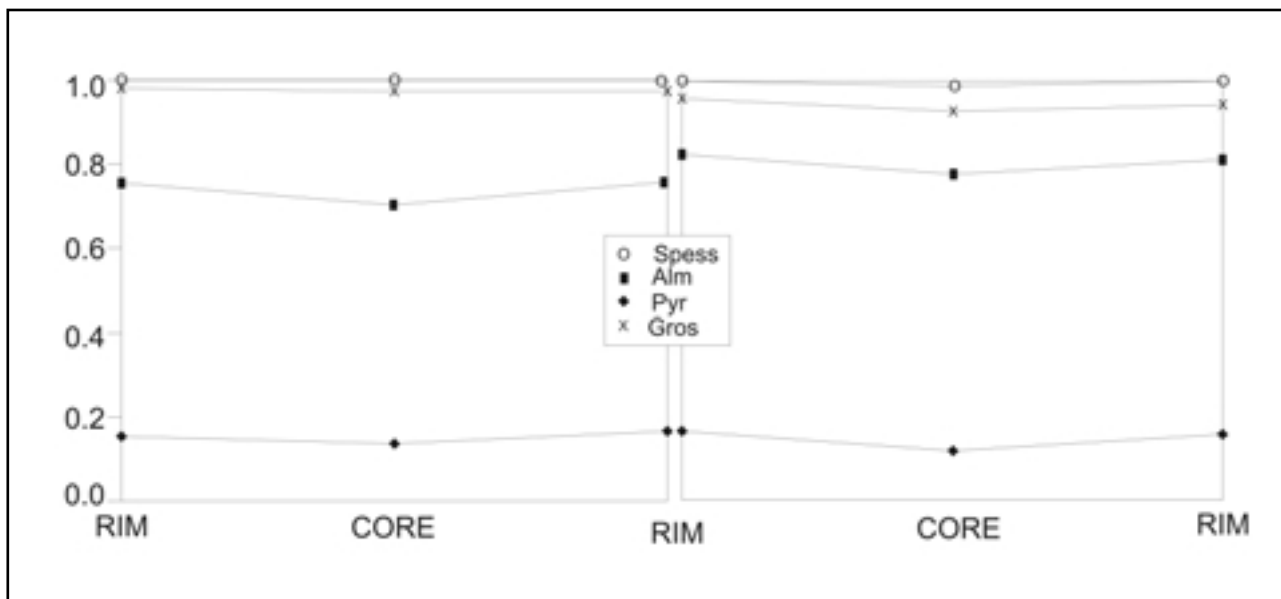
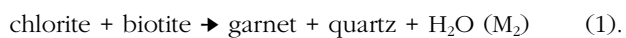


Figure 8. Representative compositional zoning profiles across individual garnet grains from sample SB06 and SB12.

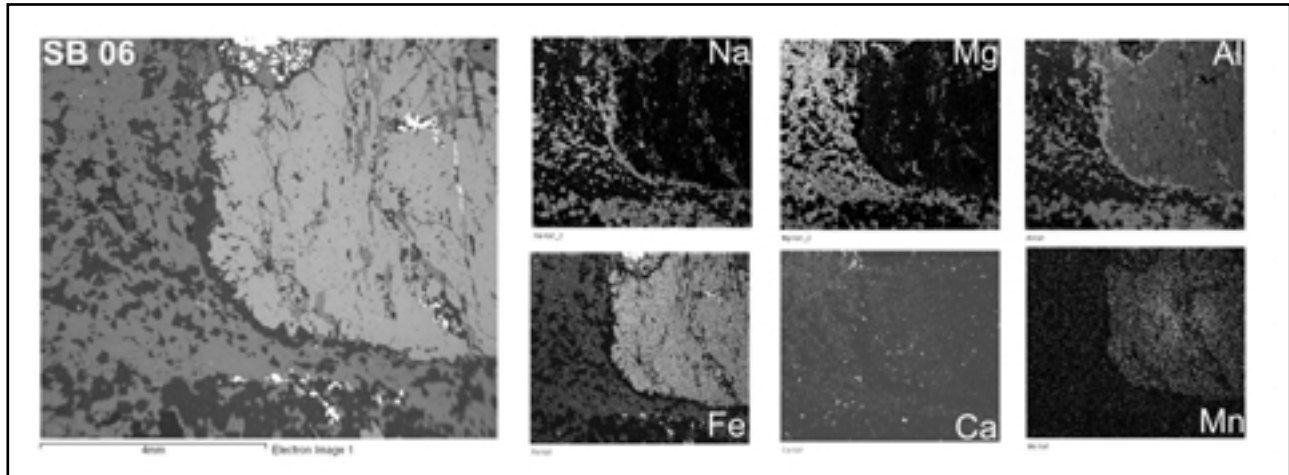
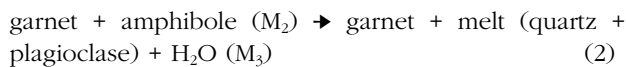


Figure 9. Elemental map for sample SB06 showing the distribution of Na, Mg, Al, Fe, Ca, Mn found in the sample.

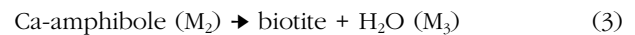
Plagioclase and quartz leucosomes form coronas around the garnet porphyroblasts from which decompression melting (Johnston *et al.*, 2001; Figure 5A) via the reaction:



is inferred. The garnet grains are typically anhedral, deformed and commonly replaced by elongate brown biotite, altered plagioclase (partly altered to sericite) and quartz along cracks. These minerals also occur as inclusions within the garnet porphyroblasts, giving rise to a poikiloblastic texture. Plagioclase exhibits wedge-shaped and multiple albite twins and radiating extinction (Figure 5A), while elongate quartz grains (Figure 5B) have undulose extinction. We interpret these features as products of either D_3 or D_4 .

Sample SB06 contains garnets which are enveloped by a matrix of syn-kinematic, fabric-defining hornblende, plagioclase and quartz. The hornblende

laths are typically blue-green, fragmented, contain plagioclase and quartz inclusions and range in length from 1 to 1.5 mm. Sample SB12 contains relatively larger and cleaner (less inclusions and less altered) hornblende laths. In this sample biotite partially replaced hornblende according to the following breakdown reaction:



The epidote amphibolite is characterised by anhedral, light green epidote grains (Figure 5C) and symplectic epidote-quartz intergrowths interpreted to be the product of the breakdown of hornblende. In one sample (SB20) symplectic epidote and quartz forms coronas around plagioclase (Figure 5D). The hornblende, plagioclase and quartz define the regional foliation (S_2) with epidote mainly occurring in cross-cutting veinlets.

In a poorly foliated sample the hornblende laths are typically nematoblastic and display a 120° triple junction when in contact with quartz and plagioclase along grain

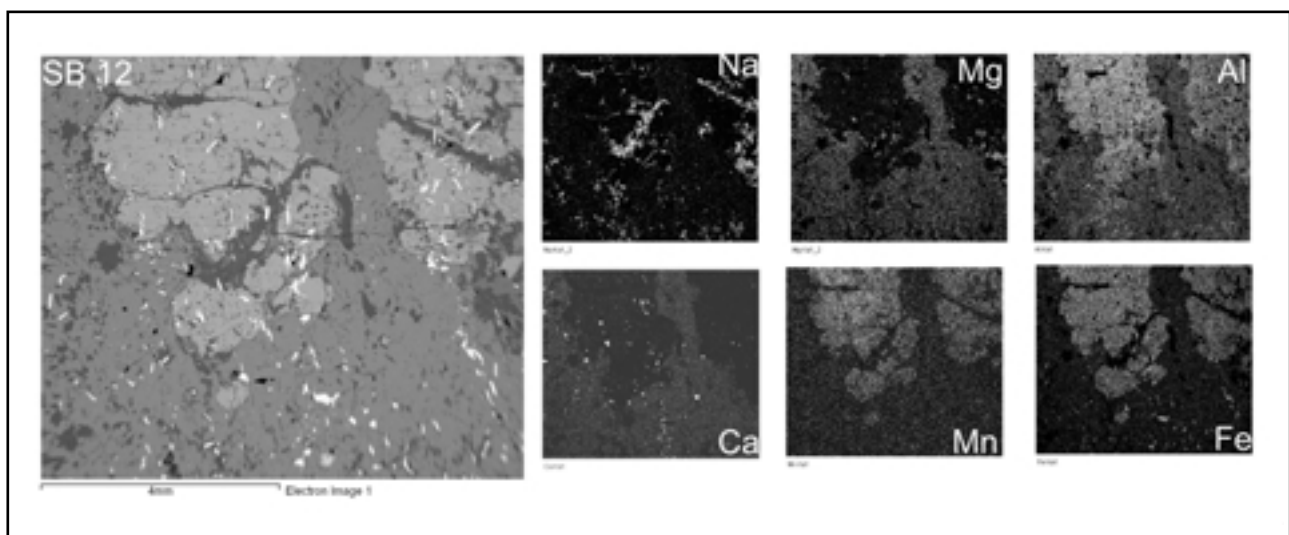


Figure 10. Elemental map for sample SB12 showing the distribution of Na, Mg, Al, Fe, Ca, Mn found in the sample.

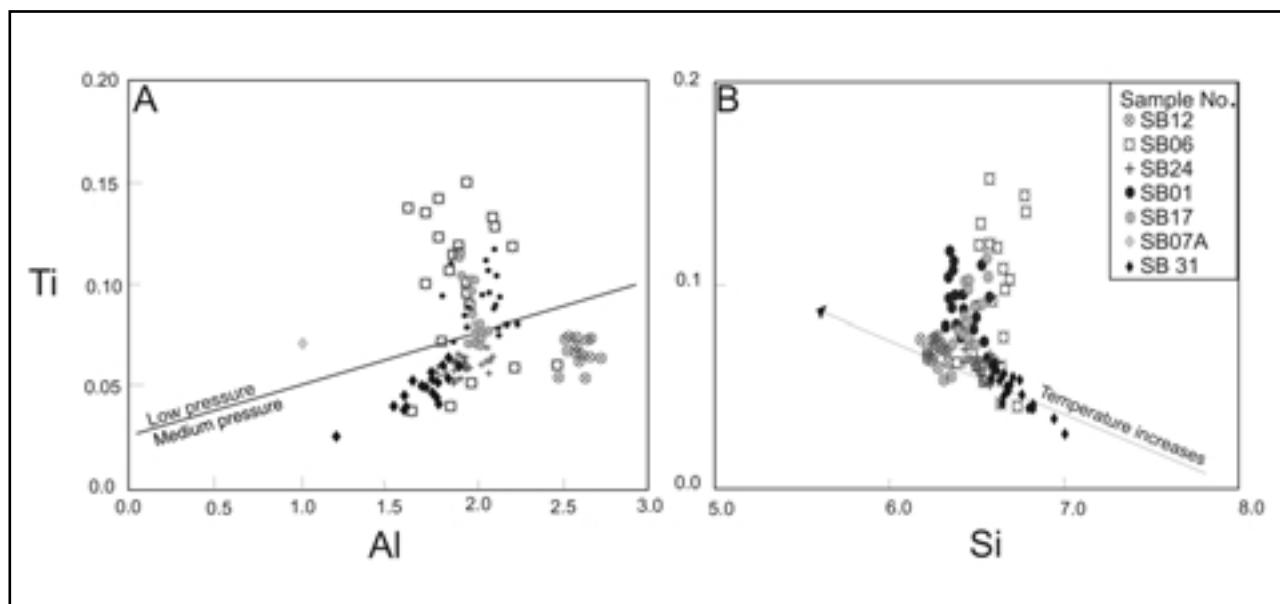


Figure 11. (A) Ti vs Al in amphibole (cations per 23 oxygens) illustrating the pressure conditions of metamorphism for the various samples with the bulk plotting in the medium pressure field. Straight line is that suggested by Hynes (1982) for distinction between low- and medium-pressure metamorphic terranes; (B) Ti vs Si (cations per 23 oxygens) indicating slightly higher temperatures for garnet amphibolite (SB12) with the bulk of the analysed samples plotting over a similar temperature range.

boundaries. In some samples, medium- to coarse-grained pleochroic poikiloblastic hornblende grains have inclusions (0.5 to 1 mm) of quartz, plagioclase and an opaque phase.

The biotite amphibolite is essentially made up of hornblende + biotite + plagioclase (partly altered to sericite) + opaque (ilmenite) (M_2) \pm secondary epidote. This lithotype shows a nematoblastic texture in which the biotite occurs as laths with a preferred orientation paralleling the regional foliation that is defined by the hornblende.

It is strongly pleochroic and reddish-brown. The biotite is commonly wrapped around flattened

quartz grains (Figure 5E), and in places, it replaced hornblende.

The mineralogically simpler amphibolite lithotype consists of hornblende + plagioclase (partly altered to sericite) + quartz \pm opaque phase (ilmenite) (M_2) \pm epidote \pm actinolite \pm biotite (M_3) and has a nematoblastic texture. The hornblende grains display perfect cleavage although, in many places, this is obscured due to their poikiloblastic appearance. Some hornblende grains are zoned with typically pale-green rims and blue-green cores. This could be a result of chemical zonation towards a more actinolitic rim and may be the result of retrograde metamorphism. The plagioclase grains were partly sericitised and some grains display undulose extinction, deformation twins (Figure 5F) and incomplete wedge-like twins.

Table 4. Representative temperatures derived from hornblende-plagioclase pairs for garnet-free amphibolites at different pressure conditions.

Sample number	Pressure (kbar)	Hbl-Pl pairs
		Temperature ($^{\circ}$ C)
Holland and Blundy (1994)		
SB01	4.5	772-834
	5.5	757-818
	6.0	750-790
SB17	4.5	736-786
	5.5	704-778
	6.0	697-763
SB24	4.5	762-838
	5.5	724-793
	6.0	717-787
SB31	4.5	711-759
	5.5	697-744
	6.0	693-789

Table 5. Representative temperature conditions for the garnetiferous amphibolites using hornblende-plagioclase and hornblende-garnet pairs.

Sample number	Pressure (kbar)	Hbl-Pl pairs
		Temperature ($^{\circ}$ C)
Holland and Blundy (1994)		
SB06	4.5	840-859
	5.5	754-840
	6.0	744-825
Hbl-Pl pairs		
Temperature ($^{\circ}$ C)		
Graham and Powell (1984)		Perchuk <i>et al.</i> (1985)
SB06	572-675	502-581
SB12	406-693	440-721

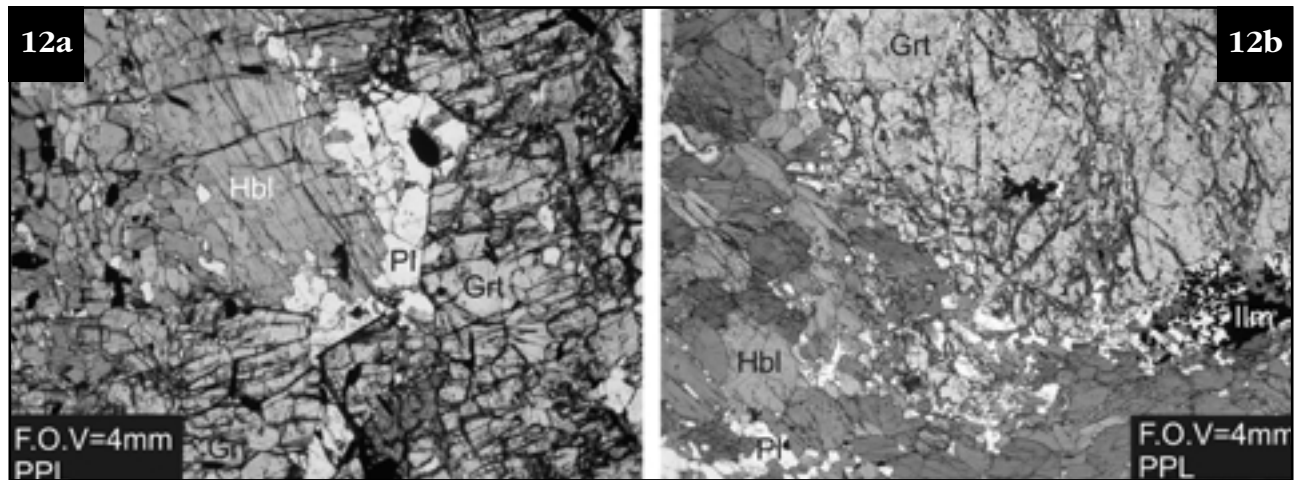


Figure 12. (a) Garnet-hornblende-plagioclase mineral assemblage observed in sample SB12; (b) hornblende-plagioclase mineral assemblage observed in sample SB06.

A total of 230 electron microprobe analyses were conducted on amphibole, plagioclase and garnet grains. Representative mineral analyses for each sample are given in Tables 2 and 3.

Amphibole makes up between 20 and 60 volume % and it shows little compositional variation. Following the nomenclature of Leake *et al.* (1987) and assuming all Fe as Fe^{2+} , the amphibole compositions (Table 2) correspond to magnesianhornblende to tschermakite (Figure 6).

Two chemically distinct varieties of plagioclase (modal proportion: 10 to 40 volume %) were identified (Figure 7). The first group ranges in composition from An_{80} to An_{90} and the second group has a composition of An_{15} to An_{50} . The orthoclase contents are less than 2%.

The plagioclase in the garnetiferous amphibolite (SB06 and SB12) plot in the bytownite field (An_{80} to An_{90}) and generally occurs as rims around garnet. However, some grains are more sodic with An_{15-50} . The anorthite-rich variety represents peak metamorphic plagioclase, whereas the more sodic variety is interpreted as a retrograde phase.

Garnet makes up between 10 and 45 volume % of the amphibolites and is almandine-rich ($X_{Alm} = 57$ to 66%, $X_{Grs} = 13$ to 28%, $X_{Pyr} = 12$ to 19% and $X_{Sps} = 1$ to 7%). Garnet profiles (Figure 8A and B) for samples SB06 and SB12 show slight zonation regardless of size and orientation of the analysed grain. In sample SB06 the X_{Alm} and X_{Pyr} proportions decrease slightly from rim to core with a corresponding increase in X_{Grs} . However, in SB12 an opposite trend is observed with a decrease

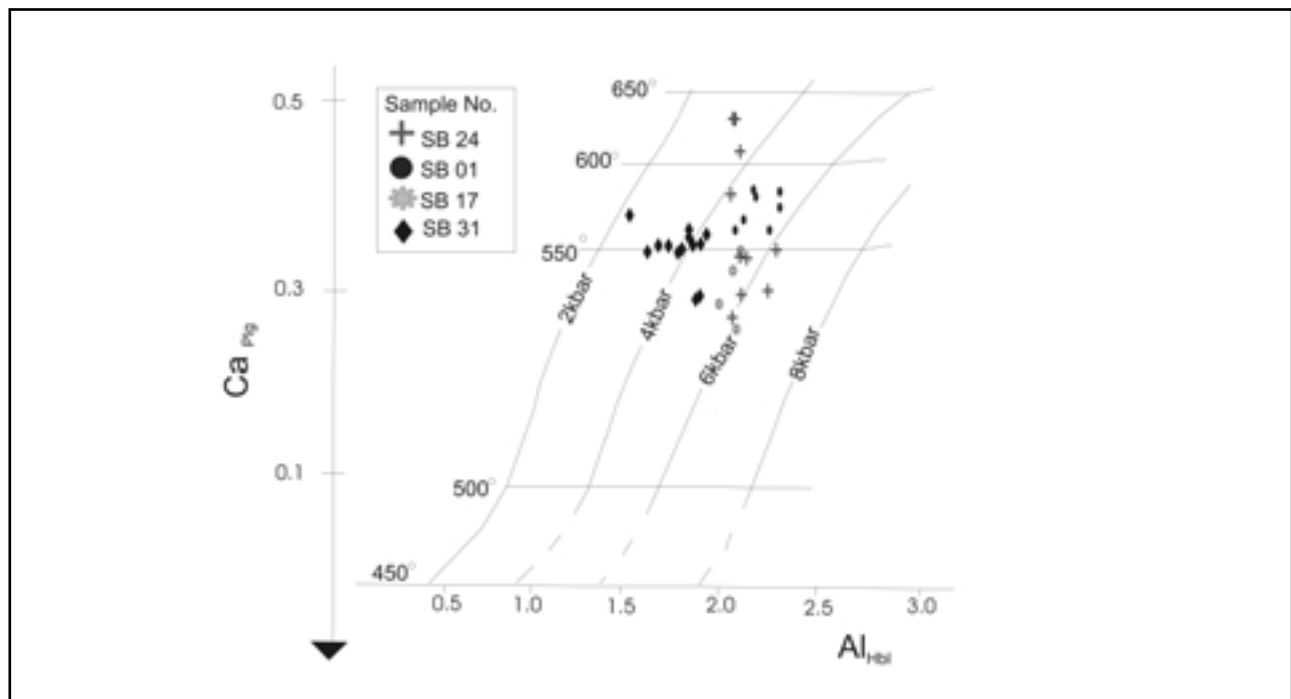
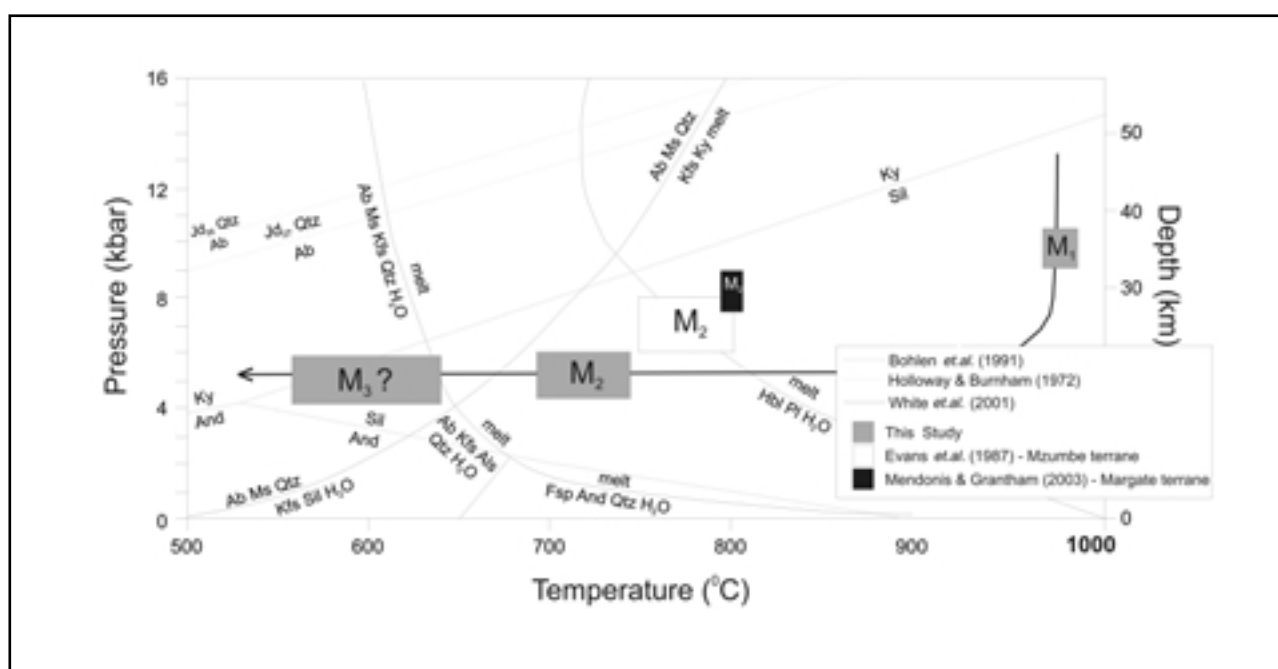


Figure 13. Pl-Hbl geothermometer after Pluysnina (1982) showing P-T plot for amphibolites from the Tugela Terrane.

Table 6. Representative pressure calculated for the analyzed samples using amphibole-garnet-plagioclase barometers of Hammarstrom and Zen (1980), Hollister *et al.* (1980) and Johnson and Rutherford (1989).

Sample Number	Pressure (kbar)		
	Hammarstrom and Zen (1980)	Hollister <i>et al.</i> (1980)	Johnson and Rutherford (1980)
SB01	5.5-6.4	5.8-6.1	4.9-6.1
SB06	4.7-6.7	4.9-6.5	5.2-7.0
SB12	6.3-8.6	6.8-8.0	5.7-7.0
SB17	5.7-6.0	6.4-7.0	5.1-5.8
SB24	5.4-5.8	5.7-6.8	4.9-5.7
SB31	4.9-5.2	4.1-5.6	4.4-4.8

**Figure 14.** Suggested pressure-temperature-time path for the amphibolites from the Tugela Terrane. Al_2SiO_5 equilibria, granitic and basaltic solidus curves shown for reference.

in X_{Grs} from rim to core and a corresponding increase in X_{Pyr} and X_{Spss} , at constant X_{Alm} .

Further evidence for the weakly zoned nature of the garnet grains is observed in elemental maps (Figure 9) produced using a scanning electron microscope. Mapping was carried out to highlight the distribution of the following elements: Mg, Na, Al and Fe within the matrix and garnet grains. The garnet map also shows that there are high concentrations of Al, Na and Si concentrated around the garnet. This is attributed to the corona of quartz and feldspar as observed both at outcrop and thin-section scale. The matrix mainly shows a high concentration of Mg, which is hosted within the dominant hornblende that characterises these rocks.

The garnet grains in sample SB12 are highly fractured and anhedral (Figure 10). They are almandine-rich (Figure 10) and contain abundant inclusions of hornblende, plagioclase and ilmenite. The fractures in the garnet grains are filled largely by Na-rich plagioclase.

Geothermobarometry

Apart from relics of diopside, the preserved equilibrium mineral assemblage, defining S_2 in the pre-tectonic mafic

rocks, consists of hornblende + plagioclase + quartz \pm garnet \pm biotite \pm ilmenite. Hynes (1982) pointed out that at low pressure amphiboles have higher Ti contents than those formed at medium pressure at the same Al level. The amphiboles from this study plot across the Ti vs. Al diagram with a greater cluster in the medium pressure field (Figure 11A). Sample SB06 plots in the low-pressure field, which could be a result of partial diffusional resetting due to decompression melting, indicated by decompression coronas around garnet. The amphibole grains in the garnet amphibolite have high Ti concentrations, which correspond to upper amphibolite-facies conditions (Figure 11B; Shido and Miyashiro, 1959; Binns, 1965; Bard, 1970; Raase, 1974; El-Naby *et al.*, 2000).

The peak metamorphic conditions (M_{regional}/M_2) were constrained further by means of hornblende-plagioclase (Holland and Blundy, 1994), garnet-hornblende (Graham and Powell, 1984) and plagioclase-hornblende (Plyusnina, 1982) geothermometry as well as garnet-hornblende-plagioclase-quartz geobarometry (Hammarstrom and Zen, 1980; Hollister *et al.*, 1987; Johnson and Rutherford, 1989; Kohn and Spear, 1990).

The edenite-tremolite geothermometer of Holland and Blundy (1994) was applied to all samples because of the presence of small amounts of quartz in the equilibrium assemblage. This geothermometer is suitable for a temperature range of 500° to 1100°C, plagioclase compositions of $An_{<92}$, and <7.8 Si atoms per amphibole formula unit. These conditions are fulfilled in the case of the samples studied. In each sample, P-T estimates were made for several microdomains in which the relevant phases appear in textural equilibrium (Figure 12). For an assumed pressure range of 4.5 kbar to 6 kbar in accordance with medium-P metamorphism that is broadly indicated in Figure 11A, a temperature range between 693 and 770°C was calculated (Table 4) for the garnet-free amphibolites. Higher temperatures (750 to 850°C) were obtained from the hornblende-plagioclase geothermometer for garnetiferous amphibolite, but lower temperatures from garnet-hornblende geothermometry (Graham and Powell, 1984) (Table 5). Using the experimental hornblende-plagioclase geothermobarometer of Plyusnina (1982; Figure 13), the garnet-free epidote-bearing samples plot between 550 and 650°C with corresponding pressures of between 3.5 and 6 kbar.

Geobarometric calculations were limited by the lack of suitable pairs. The Al-in amphibole geobarometer (Hammarstrom and Zen, 1980; Hollister *et al.*, 1987; Johnson and Rutherford, 1989) yielded pressures between 4.1 and 6.7 kbar (Table 6). The amphibole-garnet-plagioclase barometer (Kohn and Spear, 1990) gave a pressure of 4.7 at an assumed temperature of 550°C which is in good agreement with the above calculated P-T conditions using the method of Plyusnina (1982).

For the garnet-bearing samples, the temperatures calculated from hornblende-plagioclase geothermometry are at least 744 °C, which is at variance with those obtained from the garnet-hornblende thermometry (see Table 5). This discrepancy between the two methods could be a result of partial diffusional resetting of plagioclase during decompression melting as a result of uplift (see reaction 2), implying that the plagioclase compositions represent a younger, retrograde overprint and are not part of the equilibrium mineral assemblage.

Combining the results of the various geothermobarometers, an overall temperature range for M_2 conditions of between 693 and 750°C and a pressure range of 4.5 to 6 kbar is suggested. However, it must be noted that a lower temperature range of between 550 to 650°C and similar pressures have also been calculated combining the data produced using the methods of Plyusnina (1982) and Kohn and Spear (1990). These lower temperatures could represent possible M_3 conditions, but textural disequilibrium between chlorite, epidote and earlier formed minerals does not permit the use of geothermobarometry to quantify M_3 P-T conditions in detail.

P-T Path

This study and previous workers (Bisnath, 2000; Johnston *et al.*, 2003) have documented three metamorphic stages (M_1 - M_2 - M_3) within the rocks of the Tugela Terrane. Evidence for the M_1 event is preserved in thin section as an internal fabric (S_1) of inclusion trails in garnet porphyroblasts (Bisnath, 2000; Johnston *et al.*, 2003). Johnston *et al.* (2003) documented that the clinopyroxene-bearing amphibolites are, at the least, transitional between upper amphibolite- and granulite-facies metamorphism (Harley, 1989; Spear and Cheney, 1989), requiring minimum temperatures of 700°C. At low pressures (~2 kbar) clinopyroxene amphibolites develop at temperatures about 30°C lower than two-pyroxene granulites. Thus the lack of orthopyroxene in the metabasites and banded grey gneisses may indicate that temperatures were below the orthopyroxene stability field. However, this is inconsistent with migmatitisation of mafic igneous rocks, which requires temperatures of approximately 1000°C (Harley, 1989; Yardley, 1991). Alternatively, the lack of orthopyroxene may be indicative of high pressure granulite-facies metamorphism. At pressures above 9 kbars, orthopyroxene breaks down, giving rise to garnet (with an elevated grossular component), diopside and quartz (Yardley, 1991), consistent with the S_2 mineral paragenesis. High-pressure granulite-facies metamorphism is consistent with the granoblastic texture of the diopside amphibolites, the brown colour of the hornblende grains, the presence of perthitic potassium feldspar porphyroblasts, the replacement of biotite by potassium feldspar, and the migmatitisation of the mafic igneous rocks, all of which are commonly associated with granulite facies metamorphism (Yardley, 1991). Therefore it is suggested, that the presence of relic clinopyroxene represents the remnants of M_1 metamorphism and not M_2 .

The second metamorphic stage (M_2) was a retrogressive event leaving behind only hints of an earlier granulite-facies event. M_2 gave rise to the dominant minerals and foliation (S_2) in the rocks of the study area. The new geothermobarometric data indicate that the P-T conditions for M_2 were between 693 and 750°C with a pressure in the range of 4.5 to 6 kbar (Figure 14).

The final metamorphic stage observed within the analysed samples (M_3) is also interpreted as a retrogressive event associated with the D_3 event during exhumation. Retrograde metamorphism involved formation of biotite after hornblende, the replacement of hornblende by epidote and the sericitisation of plagioclase. In some areas, actinolite replaced hornblende along the grain margins. The calculated T-P conditions for M_3 are 550 to 600°C and 4 to 6 kbar.

No major differences were noted in the tectono-thermal regimes in which the rock types making up the Tugela Terrane were deformed. This is in agreement with a recent model by McCourt *et al.* (2006) in which the present components of the Tugela Terrane were

assembled during an accretionary event (D₂) between 1208 ± 5 Ma and 1161 ± 9 Ma. Syn- to post-accretion uplift (D₃) resulted in emplacement of the accreted units, as a single package, onto the margin of the Kaapvaal Craton. This uplift took place between 1155 ± 6 Ma and 1135 ± 9 Ma (McCourt *et al.*, 2006); was accommodated by northeast-vergent folds and thrusts and produced the present structural architecture of the Tugela Terrane. The accretion of the Mzumbe-Margate Terranes onto the Tugela-Kaapvaal margin occurred at ~1.08 Ga but this event is not reflected in the P-T history of the rocks in the Tugela Terrane.

Acknowledgments

A. Walliser and M. Atanasova are thanked for their assistance with electron microprobe and scanning electron microprobe analyses at the Council for Geoscience, Pretoria. S. Pillay is thanked for petrographic section preparation at the University of KwaZulu-Natal. The Council for Geoscience is thanked for financial assistance, funding SBNB Honours programme at the UKZN and giving the authors permission to publish their new findings. An earlier version of the manuscript benefitted from constructive reviews by Stephen Johnston, Bob Thomas and Geoff Grantham for which the authors are grateful.

References

- Arima, M., Tani, K., Kawate, S. and Johnston, S.T. (2001). Geochemical characteristics and tectonic setting of metamorphosed rocks in the Tugela terrane, Natal belt, South Africa. *Memoirs of the National Institute of Polar Research*, **55**, pp 1-39.
- Bard, J.P. (1970). Composition of hornblende formed during the Hercynian Progressive metamorphism of the Aracena metamorphic belt (southwest Spain). *Contributions to Mineralogy and Petrology*, **28**, pp 117-134.
- Binns, R. A. (1965). The mineralogy of metamorphosed basic rocks from the Willyama Complex, Broken Hill district, New South Wales, Part I. Hornblendes. *Mineralogical Magazine*, **35**, pp 306-326
- Bisnath, A. (2000). Geology of the Tugela Group Rocks in the Nsuze River Valley, Tugela Terrane, Natal Belt, South Africa. *Unpublished M.Sc. Thesis, University of Durban-Westville, South Africa*, 110p.
- Bohlen, S.R., Montana, A. and Kerrick, D.M. (1991). Precise determination of the equilibria kyanite <=> sillimanite and kyanite <=> andalusite and a revised triple point for Al₂SiO₅ polymorphs. *American Mineralogist*, **76**, 677-680.
- Duncumb, P. and Reed, S.J.B. (1968). Quantitative electron probe microanalysis. In: K. F. J. Heinrich (Editor), *National Bureau of Standards Special Publication*, **289**, 144-166.
- El-Naby H. A., Frisch W. and Hegner E. (2000). Evolution of the Pan-African Wadi Haimur Metamorphic Sole, eastern Desert, Egypt. *Journal of Metamorphic Geology*, **18**, 639-651.
- Evans, M.J., Eglinton, B.M., Kerr, A. and Saggerson, E.P. (1987). The geology of the Proterozoic rocks around Umzinto, southern Natal, South Africa. *South African Journal of Geology*, **90**, 471-488.
- Graham, C. M. and Powell, R. (1984). A garnet-hornblende geothermometer: calibration, testing and application to the Pelona Schist, Southern California. *Journal of Metamorphic Geology*, **2**, 13-31.
- Hammarstrom J.M. and Zen, E. A. (1980). Aluminum in Hornblende: An empirical igneous geobarometer. *American Mineralogist*, **71**, 1297-1313.
- Harley, S.L. (1989). The origins of granulites: a metamorphic perspective. *Geological Magazine*, **126**, 215-247.
- Harmer, R.E. (1979). Pre-Cape Geology of the Tugela Valley north of Kranskop, Natal. *Unpublished M.Sc. Thesis, University of Natal, Durban, South Africa*, 235pp
- Heinrich, K.F.J. (1968). Advances in X-ray micro-analysis, **11**, Plenum Press New York. United States of America.
- Holland, T. and Blundy, J. (1994). Non-ideal interactions in calcic amphiboles and their bearing on amphibole-plagioclase thermometry. *Contributions to Mineralogy and Petrology*, **116**, 433-447.
- Hollister, L.S., Grissom, G.C., Peters, E.K., Stowell, H.H. and Sisson V.B. (1987). Confirmation of the empirical correlation of Al in hornblende with pressure solidification of Calc-alkaline plutons. *American Mineralogist*, **72**, 231-239.
- Holloway J.R. and Burnham C.W. (1972). Melting relations of basalt with equilibrium water pressure less than total pressure. *Journal of Petrology*, **13**, 1-29.
- Hynes, A. (1982). A comparison of amphiboles from medium oceanic and lowpressure metabasites. *Contributions to Mineralogy and Petrology*, **81**, 119-125.
- Jacobs, J., Thomas, R.J. and Weber, K. (1993). Accretion and indentation tectonics at the southern edge of the Kaapvaal craton during the Kibaran/Grenville orogeny. *Geology*, **21**, 203-206.
- Jacobs, J. and Thomas, R.J. (1994). Oblique collision at about 1.1 Ga along the southern margin of the Kaapvaal continent, south-east Africa. *Geologische Rundschau*, **83**, 322-333.
- Johnson, M. C. and Rutherford, M. J. (1989). Experimental calibration of the aluminum-in-hornblende geobarometer with application to the Long Valley Caldera (California) volcanic rocks. *Geology*, **17**, 839-841.
- Johnston, S.T., Arima, M., Kawate, S., Shiraishi, K., Kimura, J. and McCourt, S., 1998. The Kontongweni Tonalite, Tugela Terrane, southeastern Africa: The plutonic root of a Grenvillian Oceanic Arc. *GSA Abstracts, Annual Meeting Toronto, Canada*, 256pp.
- Johnston, S.T., Armstrong, R., Heaman, L., McCourt, S., Mitchell, A., Bisnath, A. and Arima, M. (2001). Preliminary U-Pb geochronology of the Tugela terrane, Natal belt, eastern South Africa. *Memoirs of the National Institute of Polar Research*, **55**, 40-58.
- Johnston, S.T., McCourt, S., Bisnath, A. and Mitchell, A. A. (2003). The Tugela Terrane, Natal belt: Kibaran magmatism and tectonism along the southeast margin of the Kaapvaal Craton. *South African Journal of Geology*, **106**, 85-97.
- Kohn, M.J. and Spear, F.S. (1990). Two new geobarometers for garnet amphibolites, with applications to southeastern Vermont. *American Mineralogist*, **75**, 89-96.
- Kretz, R. (1983). Symbols for rock forming minerals. *American Mineralogist*, **68**, 277-279.
- Leake, B.E., Woolley, A.R., Arps, C.E.S., Birch, W.D., Gilbert, M.C., Grice, J.D., Hawthorne, F.C., Kato, A., Kisch, H.J., Krivovichev, V.G., Linthout, K., Laird, J., Mandarion, J., Maresch, W.V., Nickel, E.H., Rock, N.M.S., Schumacher, J.C., Smith, D.C., Stephenson, N.C.N., Ungaretti, L., Whittaker, E.J.W. and Youzhi, G. (1987). Nomenclature of Amphiboles: Report of the Subcommittee on Amphiboles of the International Mineralogical Association Commission on New Minerals and Mineral Names. *Mineralogical Magazine*, **61**, 295-321.
- Matthews, P.E. (1972). Possible Precambrian obduction and plate tectonics in southeastern Africa. *Nature*, **240**, 37-39.
- Matthews, P.E. (1981). Eastern or Natal sector of the Namaqua-Natal Mobile belt in southern Africa. In: D.R. Hunter (Editor), Precambrian of the southern hemisphere. Elsevier, Amsterdam, The Netherlands, 705-725.
- Matthews, P.E. and Charlesworth, E.G. (1981). A geological review of the northern margin of the Proterozoic Namaqua-Natal mobile belt in Natal. *Geocongress '81. Guidebook, Geology Society of South Africa*, 83pp.
- McCourt, S; Armstrong, R.A., Grantham, G.H. and Thomas, R.J. (2006). Geology and evolution of the Natal belt, South Africa. *Journal of African Earth Sciences*, **46**, 71-92.
- Mendonidis, P. and Grantham, G.H. (2003). Petrology, origin and metamorphic history of proterozoic-aged granulites of the Natal Metamorphic Province, southeastern Africa. *Gondwana Research*, **6**, 607-628.
- Philibert J. (1963). A method of calculating the absorption correction in electron probe microanalysis, In: H.H. Pattee, V.E. Cosslett and Arne Engström (Editors). Third International Symposium, X-ray optics and, X-ray microanalysis. Academic Press, New York, United States of America, 379-392.
- Plyusnina, L.P. (1982). Geothermometry and geobarometry of plagioclase-hornblende bearing assemblages. *Contributions to Mineralogy*

- and *Petrology*, **80**, 140-146.
- Reynolds I.M. (1986). The mineralogy and ore petrography of the Bushveld titaniferous magnetite-rich layers. In: C.R. Anhaeusser and S.Maske (Editors), Mineral Deposits of Southern Africa, *Geological Society of South Africa*, 1267-1286.
- Raase, P. (1974). Al and Ti contents of hornblende, indicators of pressure and temperature of regional metamorphism. *Contributions to Mineralogy and Petrology*, **45**, 231-236.
- Reed, S.J.B. (1965). Characteristic fluorescence correction in electron-probe microanalysis. *British Journal of Applied Physics*, 16pp.
- Shido, F. and Miyashiro, A. (1959). Hornblende of basic metamorphic rocks. *Journal of the Faculty of Science, Tokyo University, Japan, Section II*, **12**, 85-102.
- Smalley, T.J. (1980). Structure and metamorphism of the Tugela Group within the northern zone of the Natal-Mobile Belt. *Unpublished Ph.D Thesis, University of Natal, Durban, South Africa*, 220pp
- Spear, F.S. and Cheney, J.T. (1989). A petrogenetic grid for pelitic schists in the system SiO_2 - Al_2O_3 - FeO - MgO - K_2O - H_2O . *Contributions to Mineralogy and Petrology*, **101**, 149-164.
- Thomas R.J. (1989a). Preface to the special issue on the Proterozoic rocks of the natal structural and Metamorphic Province. *South African Journal of Geology*, **92**, 339-351.
- Thomas, R.J. (1989b). A tale of two tectonic terranes: *South African Journal of Geology*, **92**, 306-321.
- Thomas, R.J. and Eglington, B.M. (1990). A Rb-Sr, Sm-Nd and U-Pb zircon isotopic study of the Mzombe Suite, the oldest intrusive granitoid in southern Natal, South Africa. *South African Journal of Geology*, **93**, 761-765.
- Thomas, R.J., von Veh, M.W. and McCourt, S. (1993). The tectonic evolution of southern Africa: an overview. *Journal of African Earth Science*, **16**, 5-24.
- Thomas, R.J., Agenbacht, A.D., Cornell, D.H. and Moore, J.M. (1994). The Kibaran of Southern Africa: Tectonic evolution and metallogeny. *Ore Geology Reviews*, **9**, 131-160.
- Thomas, R.J., Jacobs, J., Falter, M. and Jessberger, A. (1996). K-Ar and Ar-Ar dating of mineral separates from the Natal metamorphic province. *Geological Survey of South Africa Annual Technical Report*, **95**, 52-56.
- White, R.W., Powell, R. and Holland, T.J.B. (2001). Calculations of partial melting Equilibria in the system Na_2O - CaO - K_2O - FeO - MgO - Al_2O_3 - SiO_2 - H_2O (NCKFMASH). *Journal of Metamorphic Petrology*, **19**, 139-153.
- Wuth, M.G. and Archer, P.D. (1986). Chromite mineralization at Sithilo, northern Zululand. In: C.R. Anhaeusser and S. Maske (Editors), Mineral Deposits of Southern Africa, *Geological Society of South Africa*, 1689-1694.
- Yardley, B.W.D. (1991). An Introduction to Metamorphic Petrology. *John Wiley and Sons Inc, New York, United States of America*, 248pp.

Editorial handling: L.D. Ashwal